Comparative investigation of the reaction mechanisms of the organophosphate-degrading phosphotriesterases from Agrobacterium radiobacter (OpdA) and Pseudomonas diminuta (OPH)

ARTICLE *in* JBIC JOURNAL OF BIOLOGICAL INORGANIC CHEMISTRY · AUGUST 2014

Impact Factor: 2.54 · DOI: 10.1007/s00775-014-1183-9 · Source: PubMed

9 AUTHORS, INCLUDING:

Marcelo Pedroso
University of Queensland
6 PUBLICATIONS **19** CITATIONS
SEE PROFILE

Margaret C Carpenter
Dartmouth College
3 PUBLICATIONS **10** CITATIONS
SEE PROFILE

Gerhard Schenk
University of Queensland
157 PUBLICATIONS **2,613** CITATIONS
SEE PROFILE

J Biol Inorg Chem
DOI 10.1007/s00775-014-1183-9

ORIGINAL PAPER

Comparative investigation of the reaction mechanisms of the organophosphate-degrading phosphotriesterases from *Agrobacterium radiobacter* (OpdA) and *Pseudomonas diminuta* (OPH)

Marcelo M. Pedroso · Fernanda Ely · Nataša Mitić · Margaret C. Carpenter · Lawrence R. Gahan · Dean E. Wilcox · James L. Larrabee · David L. Ollis · Gerhard Schenk

Received: 15 June 2014 / Accepted: 30 July 2014

Abstract Metal ion-dependent, organophosphate-degrading enzymes have acquired increasing attention due to their ability to degrade and thus detoxify commonly used pesticides and nerve agents such as sarin. The best characterized of these enzymes are from *Pseudomonas diminuta* (OPH) and *Agrobacterium radiobacter* (OpdA). Despite high sequence homology (>90 % identity) and conserved metal ion coordination these enzymes display considerable variations in substrate specificity, metal ion affinity/preference and reaction mechanism. In this study, we highlight the significance of the presence (OpdA) or absence (OPH) of an extended hydrogen bond network in the active site of these enzymes for the modulation of their catalytic properties. In particular, the second coordination sphere residue in position 254 (Arg in OpdA, His in OPH) is identified as a crucial factor in modulating the substrate preference and binding of these enzymes. Inhibition studies with fluoride also support a mechanism for OpdA whereby the identity of the hydrolysis-initiating nucleophile changes as the pH is altered. The same is not observed for OPH.

Keywords Binding affinity · Calorimetry · Enzyme kinetics · Magnetic circular dichroism · Site-directed mutagenesis

Electronic supplementary material The online version of this article (doi:10.1007/s00775-014-1183-9) contains supplementary material, which is available to authorized users.

M. M. Pedroso · F. Ely · L. R. Gahan · G. Schenk (✉)
School of Chemistry and Molecular Biosciences, The University of Queensland, St. Lucia, QLD 4072, Australia
e-mail: schenk@uq.edu.au

N. Mitić
Department of Chemistry, National University of Ireland, Maynooth, Maynooth, Co. Kildare, Ireland

M. C. Carpenter · D. E. Wilcox
Department of Chemistry, Dartmouth College, Hanover, NH 03755, USA

J. L. Larrabee
Department of Chemistry and Biochemistry, Middlebury College, Middlebury, VT 05753, USA

D. L. Ollis
Research School of Chemistry, Australian National University, Canberra, ACT 0200, Australia

Introduction

Organophosphorus (OP) compounds have been used worldwide as pesticides, in particular since the end of the Second World War, allowing the rapid expansion of agriculture [1]. However, the continuous and excessive use of these pesticides has resulted in soil and water contamination. OP compounds are generally stable molecules and possess high toxicity, especially for mammalian organisms [2]. Some OP compounds act as nerve agents and are classified as weapons of mass destruction (e.g., sarin, VX) [3]. The increasing application of OP pesticides has triggered some microorganisms to acquire (evolve) the enzymatic machinery to use OP compounds as a source for phosphorous [4, 5]. The best studied OP-degrading enzymes to date are from *Pseudomonas diminuta* (OPH) [6] and *Agrobacterium radiobacter* (OpdA) [7]. OpdA is commercially available (Landguard^{TM}) and has been used successfully to remediate OP insecticide-contaminated water [8].

OpdA and OPH are highly homologous, sharing ~90 % sequence identity. Both enzymes require a dinuclear metal centre for catalysis, and their metal-binding amino acid

Published online: 08 August 2014

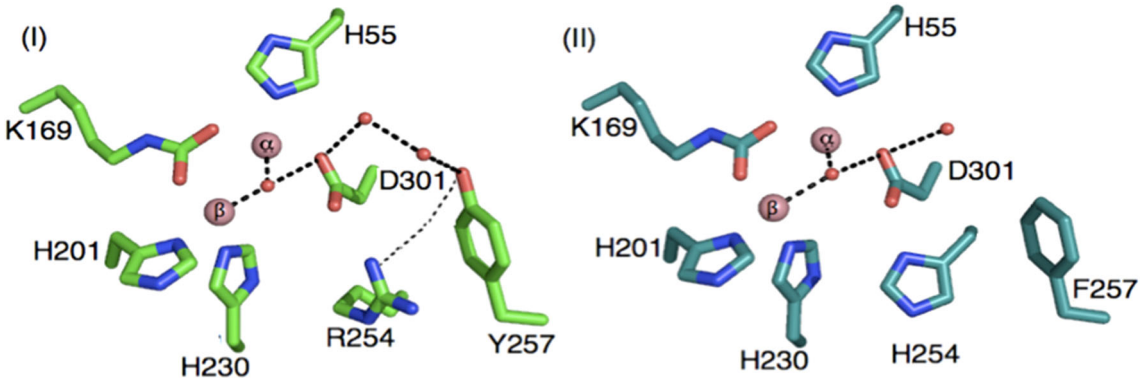

Fig. 1 Comparison of **I** wild-type OpdA (pdb accession: 2D2J [55]), **II** OPH (pdb accession: 1HZY [56]). The extensive hydrogen bonding network between μOH, Asp301, Tyr257 and Arg254 in OpdA is disrupted in OPH. Also shown is the extensive H-bond network that connects the metal ion centre to the substrate binding pocket lined by residues Arg254 and Tyr257. The distance range applied for H-bonds is 2.5–3.2 Å

side chains are identical (Fig. 1). The only variations in the vicinity of their active sites are three residues in the substrate binding pocket, i.e. Arg^{254}/His^{254}, Tyr^{257}/His^{257} and Phe^{272}/Leu^{272} in OpdA/OPH [7]. Only in OpdA are these three residues part of an extensive hydrogen bond network that connects the substrate binding pocket to the metal centre, and it has been speculated that these variations may account for the differences with respect to their substrate specificity [9–11]. For OpdA its preferred substrate is methyl-paraoxon (k_{cat} 5,652 s^{-1}; K_m 61 μM) whereas OPH prefers ethyl-paraoxon (k_{cat} 2,760 s^{-1}; K_m 50 μM). These variations may also be the reason for significant differences in the pH dependence of the catalytic parameters of the two enzymes; OpdA is active over the pH range from pH <5 to pH ~11, whereas OPH is active only above pH 6 [10, 12].

The dinuclear metal centre in OpdA and OPH is crucial for the reactivity of these enzymes, providing (1) a binding site for the substrate and (2) an activated hydroxide to initiate hydrolysis. In OPH this nucleophile is proposed to be bridging the two metal ions [12–16]. In OpdA the identity of the nucleophile may be dependent on both metal ion composition and pH [10, 17]. A caveat of previous mechanistic comparisons was that for OPH the most detailed mechanistic investigations were carried out with the Zn(II), Cd(II) or Mn(II) derivatives (including mixed-metal centres), while for OpdA the Co(II) derivative is the best characterized form [10, 12, 14, 18]. For the latter, a mechanistic model emerged that invokes a change of the hydrolysis-initiating nucleophile from a metal-bridging hydroxide at low pH to a terminally coordinated hydroxide at high pH [10, 17, 19, 20].

From the above it has become apparent that small physical changes (i.e. a limited number of amino acid variations and different metal ion compositions) may affect the function of OP-degrading enzymes significantly. To improve (and diversify) the application of such enzymes in bioremediation it is essential to gain an understanding how these changes affect the mechanism of hydrolysis, and this is the aim of the present study.

Materials and methods

Materials

The *Pfu* DNA polymerase and DpNI were purchased from Promega, and oligonucleotide primers were synthesized by Sigma Genesis. dNTPs were purchased from Bio-Rad Laboratories, and *Escherichia coli* BL21(DE3) host cells were from Novagen. All chromatographic devices were purchased from GE Healthcare. The protease inhibitor cocktail was from Roche. Ethyl-paraoxon was purchased from Sigma.

Expression and purification of OpdA and OPH

The cloning, expression and purification of both wild-type OpdA and OPH was described previously [10, 16]. The purifications yielded, on average, 12 mg OpdA and 10 mg OPH per litre of expression medium. The purity (>95 %) was confirmed by SDS-PAGE analysis, and the enzymes were stored at 4 °C until further use.

Generation of the Arg254His mutant of OpdA

The Arg254His mutant of OpdA was generated as previously described by Ely et al. [10].

Generation of Co(II) derivatives of OpdA and OPH

A 2 mL solution containing 2.5 mM ethylenediaminetetraacetic acid (EDTA), 2.5 mM 1,10-phenanthroline,

2.5 mM 2,6-pyridinedicarboxylate, 2.5 mM 8-hydroxyquinoline 5 mM sulfonic acid, 2.5 mM β-mercaptoethanol and 10 mM HEPES, pH 7.0, was added to 1 mL of 1 mg/mL enzyme. The mixture was incubated at 4 °C for 24 h, after which no more than 1.5 % residual enzyme activity remained. Enzymatic activity was monitored by recording hydrolysis of 1 mM ethyl-paraoxon in 50 mM HEPES, pH 8.0, at 405 nm ($\varepsilon = 15{,}000\ M^{-1}cm^{-1}$). The apoenzyme was separated from the chelating solution using a desalting column (10-DG Bio-Rad), which was previously equilibrated with 50 mM Tris.HCl, pH 9.0. Atomic absorption analysis confirmed the absence of metal ions. The reconstitution of enzyme activity was performed by the addition of 10 equivalents of Co(II) to the apoenzyme, followed by incubation for 24 h at 4 °C. Enzyme activity was recorded at intervals to ascertain maximum activity was reached after 24 h. The metal ion content after reconstitution (and removing the excess) was determined using atomic absorption spectroscopy and indicated the presence of stoichiometric amounts of Co(II) (i.e. 1.9–2.1).

Isothermal titration calorimetry (ITC) measurements with wild-type OpdA

All measurements were carried out using an ITC-200 MicroCal at 10 °C in 50 mM Tris.HCl buffer, pH 8.0. Both the cell and the syringe were cleaned using a 10 mM EDTA solution. Due to instability of the apo-enzyme, EDTA chelation titrations were used to investigate the metal ion affinity of OpdA. The apo-enzyme was reconstituted with 2 equivalents of metal ion [Co(II), Cd(II) or Zn(II)] and EDTA, in an identical buffer solution, was titrated into a solution of the metal-reconstituted enzyme.

ITC data analysis

The ITC data were fitted using MicroCal® Origin 7.0 software [21]. The software uses a nonlinear algorithm with minimization of χ^2, fitting the heat flow released by each injection to an equation corresponding to an equilibrium binding model. The heat of dilution was subtracted from the integrated data and a mathematical model of one (3 parameters) binding site was used to fit the integrated data. The derivations of the mathematical models used for the data fitting were described elsewhere [22, 23]. The two independent sites model provides values for the stoichiometry (n_{ITC}), change in enthalpy (ΔH_{ITC}) and binding constant (K_{ITC}) for each site. The competition binding model uses the known binding constant and binding enthalpy for one competing ligand (e.g. EDTA) to determine K and ΔH for binding to another competing ligand (e.g. OpdA). The value for the change in Gibbs free energy for each ITC titration was determined from the equilibrium constant using Eq. (1), where R (1.987 cal/mol K) is the gas constant and T is the temperature (in Kelvin). The change in entropy ($-T\Delta S^\circ$) was then determined using Eq. (2), where ΔH° is the change in enthalpy.

$$\Delta G^\circ = -RTlnK \tag{1}$$

$$\Delta G^\circ = \Delta H^\circ - T\Delta S^\circ \tag{2}$$

Enzymatic assays

All kinetic measurements were carried out with the fully reconstituted Co(II) derivatives of OpdA and OPH. In a standard assay reactions were monitored for 60 s at 25 °C with a Cary 50 Bio Varian UV–Vis spectrophotometer. Buffers were treated prior to use with Chelex resin (Bio-Rad). The pH profiles of the catalytic parameters (k_{cat}, k_{cat}/K_m) were determined using ethyl-paraoxon as substrate, with concentrations ranging from 15 μM to 3.5 mM. The pH for the assays ranged from 5.0 to 11 using a 100 mM acetate, 100 mM MES, 100 mM HEPES, 100 mM CHES, 100 mM CAPS multicomponent buffer system. Initial velocities were measured by monitoring the release of *p*-nitrophenol at the pH-independent isosbestic wavelength of 347 nm ($\varepsilon = 5{,}176\ M^{-1}\ cm^{-1}$) [12].

For the measurements of the inhibitory effect of fluoride on OpdA activity the inhibitor concentrations ranged from 0 to 1 μM. The enzyme was pre-incubated at 4 °C with fluoride for 2 h prior to initiation of the assays.

Kinetic data analysis

All data were analysed by nonlinear regression using GraphPad Prism 5 Software, Inc. Rate vs substrate concentration profiles were fitted to the Michaelis–Menten equation (Eq. 3) [24], where V_{max} represents the maximum velocity, K_m the Michaelis–Menten constant, S the substrate concentration and u the initial velocity.

$$v = \frac{V_{max} \cdot S}{(K_m + S)} \tag{3}$$

In some cases, high concentrations of substrate led to a deviation from Michaelis–Menten-type behaviour. In those cases, data were fitted to Eq. (4) where K_i represents the dissociation constant for binding of the substrate to a second, inhibitory site [24].

$$v = \frac{V_{max} \cdot S}{\left(K_m + S\left(1 + \frac{[S]}{K_i}\right)\right)} \tag{4}$$

The pH dependence of the catalytic parameters was fitted using Eq. (5), derived for a system with one relevant protonation equilibrium [24]. Here, H is the proton concentration, K represents the acid dissociation constant for either the enzyme–substrate complex (ES) or the free

enzyme (E); c is the pH-independent values of y, and y is the kinetic parameter of interest, i.e. k_{cat} or k_{cat}/K_m [24].

$$\log y = \log\left(\frac{c}{1+\frac{H}{K}}\right) \quad (5)$$

Catalytic data measured in presence of fluoride were analysed using the general inhibition equation (Eq. 6) [24]. Here, V_{max} and K_m are the maximum rate and Michaelis–Menten constant, $[S]$ and $[I]$ are the substrate and inhibitor concentrations, and K_{ic} and K_{iuc} the equilibrium dissociation constants for competitive and uncompetitive inhibitor binding, respectively.

$$\frac{1}{v} = \frac{1+\frac{[I]}{K_{iuc}}}{V_{max}} + \frac{K_m\left(\frac{[I]}{K_{ic}}\right)}{V_{max}[S]} \quad (6)$$

Magnetic circular dichroism

Co(II)-substituted OpdA and OPH samples for MCD experiments were prepared as described above; in brief, after preparation of the metal ion-free apoenzyme and reconstitution of enzymatic activity by the addition of an excess of Co(II), unbound (excess) metal ions were removed using a gel filtration column, pre-equilibrated with 50 mM HEPES, pH 8.0. Protein samples (0.87 mM for OpdA and 0.6 mM for OPH) in 50 mM HEPES buffer, pH 8.0 were diluted to a 60/40 % (v/v) mixture of glycerol/buffer and transferred to a 0.62 cm path length nickel-plated copper sample cell with quartz windows. To the same sample of OpdA 1 μL of a 400 μM fluoride solution ($[F] = 0.5$ μM) was added and the sample was measured again. The MCD system comprises a JASCO J815 spectropolarimeter, fitted with an Oxford Instruments SM4000 cryostat/magnet. Data were collected at 7.0 T and at a temperature of 1.3 or 1.4 K. Each spectrum was corrected for any natural CD by subtracting the zero-field spectrum of the sample. The resultant spectra were converted to wavenumbers and fitted to the minimum number of Gaussian peaks to achieve a satisfactory composite spectrum using the GRAMS AI software [25].

Results

Metal ion binding in wild-type OpdA: comparison to OPH

The OpdA dinuclear centre is bridged by a carboxylated lysine [9, 10, 19, 20]. The carboxylic moiety of the lysine residue is lost when the metal ions are removed; however, the dinuclear centre can be regenerated in the presence of bicarbonate [10]. For OPH it has been shown that formation of its dinuclear metal centre also depends on bicarbonate, and its average affinity for Zn(II), Co(II), and Cd(II) has been determined by equilibrium dialysis [26]. Here, ITC was employed to determine the OpdA affinity for metal ions, as well as its metal-binding thermodynamics.

Initial ITC measurements for the addition of metal ions to apo-OpdA resulted in negligible heat flow, even in the presence of carbonate concentrations as high as 200 mM. This may be due to a kinetic barrier and/or instability of the apo protein. To circumvent these issues, chelation ITC measurements involving addition of EDTA to solutions of Co(II)-OpdA, Cd(II)-OpdA and Zn(II)-OpdA (Fig. 2) were used to determine the metal affinity and metal-binding enthalpy of OpdA, as was done recently to monitor Zn(II) binding in the insulin hexamer under stabilising conditions [27]. EDTA initially chelates the more weakly bound metal ion from OpdA, and this occurs with negligible net heat. Subsequent EDTA removal of the second and more tightly bound metal ion is significantly exothermic. A fit of these data to a two independent sites model confirms the expected metal stoichiometry and provides the net chelation enthalpy for each step (Table 1) [28]. Accounting for the enthalpy associated with formation of the metal–EDTA complex under the experimental conditions allows the enthalpy for each metal ion binding to OpdA at pH 8.0 to be determined (Table 2).

The fit with the two independent sites model also provides the net chelation equilibrium constants for the two steps (Table 1). Accounting for the metal–EDTA stability ($K_{ITC} = K_{EDTA}/K_{OpdA}$) gives metal-OpdA binding constants. However, these values are not thermodynamically accurate because of the large variation in the concentration (activity) of the apo protein and chelator over the course of the titration. Further, the sharp change in titration enthalpy after one equivalent of EDTA has been added indicates that the first chelation event has an equilibrium constant that cannot be accurately determined from these data. To estimate the OpdA affinities for metal ions from the ITC data, a single-site competition binding model developed by Sigurskjold [29] and provided by MicroCal was thus used to fit the second inflection in the chelation data, which corresponds to the more tightly bound metal ion in site 1 (Figure S1–S3) [30]. This involved masking the data associated with the first chelation step, and using the known values for the binding constant (K_A) and binding enthalpy (ΔH_A) of the metal–EDTA complex, adjusted for the experimental conditions (Table 2), and using the metal-OpdA binding enthalpy (ΔH_B) from the fits with the two independent sites model (Table 1). An upper limit for the binding constant of the more weakly bound metal ion in site 2 can then be estimated from the ratio of the two values from the fit with the two independent sites model. These OpdA K_d values for pH 8.0 are indicated in Table 2.

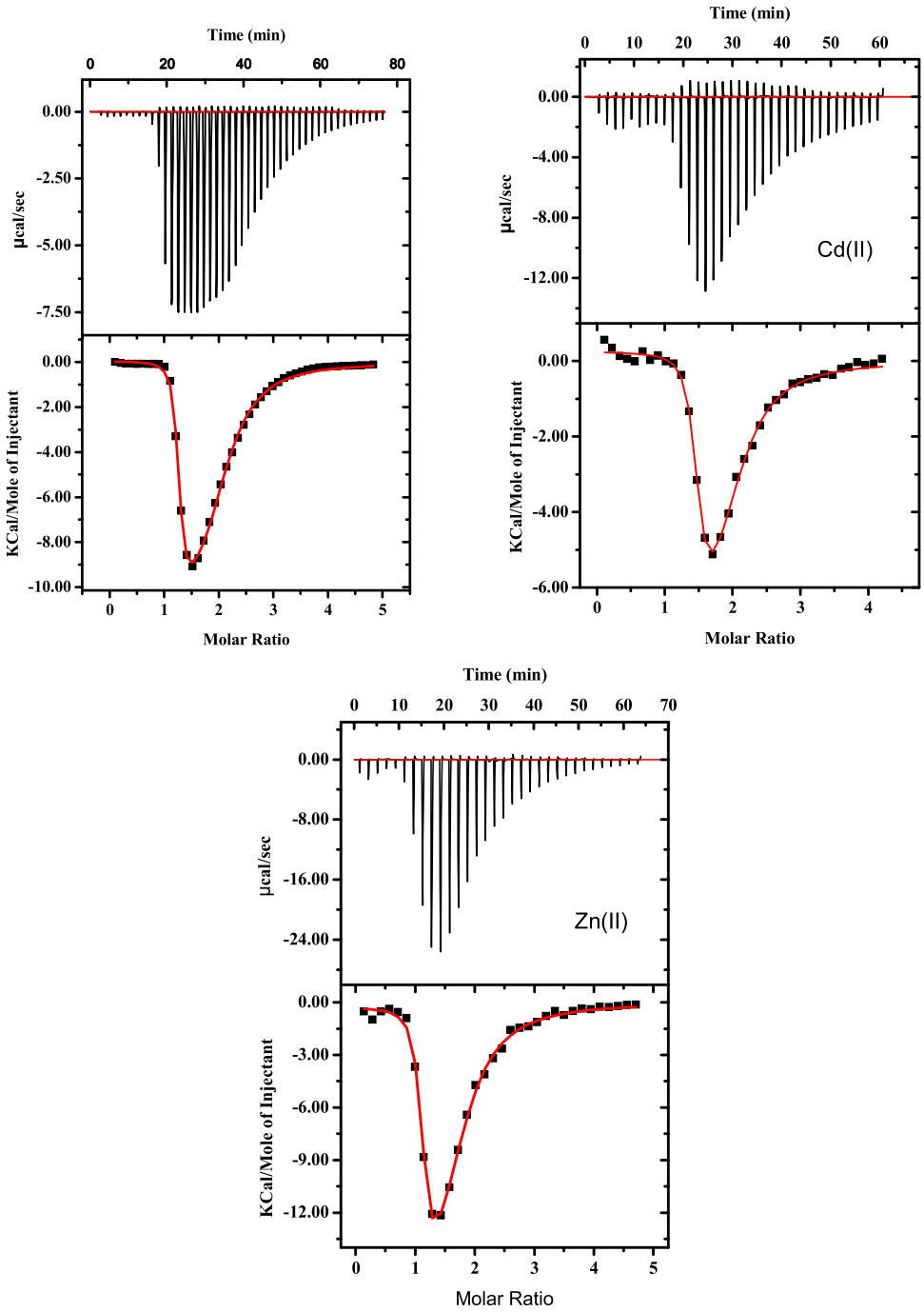

Fig. 2 ITC data for the EDTA chelation titrations of Co(II)-OpdA, Cd(II)-OpdA and Zn(II)-OpdA. Data were fitted with an independent two sites binding model with the best fit values listed in Table 1

Table 1 Best fit values for the EDTA chelation ITC data in Fig. 1 using the independent two-sites binding model

	Co(II)		Cd(II)		Zn(II)	
	Step 1	Step 2	Step 1	Step 2	Step 1	Step 2
n_{ITC}	1.22 (0.03)	0.90 (0.01)	1.3 (0.2)	0.7 (0.1)	1.1 (0.1)	0.7 (0.3)
K_{ITC}	2.5×10^6	7.3×10^3	1.0×10^6	6.7×10^3	7.3×10^5	5.5×10^3
ΔH_{ITC} (kcal/mol)	0.22	−50.7	0.26	−8.6	−0.26	−21.3

Table 2 Analysis to determine the metal-binding enthalpies and equilibrium constants for OpdA from the values in Table 1

$K^{a}_{EDTA\text{-}M}$	Co(II)		Cd(II)		Zn(II)	
	2.80×10^{13}		3.10×10^{13}		3.10×10^{13}	
$\Delta H_{EDTA\text{-}M}$ (kcal/mol)[a]	−11.3		−15.9		−10.6	
	Site 2	Site 1	Site 2	Site 1	Site 2	Site 1
$\Delta H_{OpdA\text{-}M}$ (kcal/mol)	−11.5 (0.5)	39.4 (0.2)	−16.1 (0.2)	−7.3 (0.8)	−10.3 (0.1)	10.7 (0.9)
$K_{OpdA\text{-}M}$	$<2.70 \times 10^{9}$	9.11×10^{11}	$<6.10 \times 10^{9}$	9.60×10^{11}	$<7.50 \times 10^{9}$	1.00×10^{12}
$K_{d\ OpdA\text{-}M}$ (nM)	>0.37	0.0011	>0.16	0.0010	>0.13	0.0010

[a] Determined with values from Ref. [30] corrected for the experimental conditions [28]

Table 3 OpdA metal-binding thermodynamics at pH 8.0 in 50 mM Tris

	Co(II)		Cd(II)		Zn(II)	
	Site 2	Site 1	Site 2	Site 1	Site 2	Site 1
OpdA						
$\Delta G°$ (kcal/mol)	−12.2	−15.5	−12.7	−15.5	−12.8	−15.5
$\Delta H°$ (kcal/mol)	−11.5 (0.5)	39.4 (0.2)	−16.1 (0.2)	−7.3 (0.8)	−10.3 (0.1)	10.7 (0.9)
$-T\Delta S°$ (kcal/mol)	−0.7	−54.9	3.4	−8.2	−2.5	−26.2
K_d (nM)	>0.37	0.0011	>0.16	0.0010	>0.13	0.0010
OPH[a]						
K_d (nM)	1.8		11		0.059	

[a] Average values determined by equilibrium dialysis [26]

Finally, the thermodynamics associated with metal ions binding to the two sites in OpdA at pH 8.0 were determined from these values (Table 3).

The OpdA metal affinities determined by ITC for the higher affinity site are larger than those determined previously for OPH by equilibrium dialysis [26]. However, these OPH values are the average of the affinities of the two sites. Since the ITC data can only provide an upper limit for the lower affinity site, the OpdA values determined here are not inconsistent with those determined for the similar OPH active site. In particular, the OpdA affinities for the two Zn(II) ions bracket the average value determined for OPH. The values in Table 3 indicate similar binding thermodynamics for the three metal ions at the lower affinity site 2, but significant thermodynamic differences at the higher affinity site 1. Since these measurements were made in Tris buffer, which has a large enthalpy of protonation, this could indicate metal-specific differences in (de)protonation that accompany metal binding, as found with insulin [27].

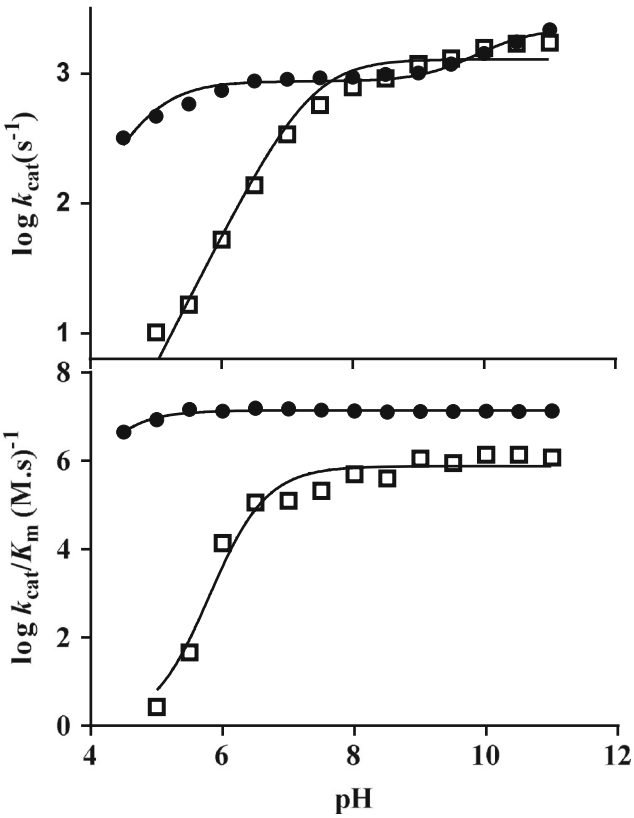

Fig. 3 The pH dependence of k_{cat} (*top*) and k_{cat}/K_m (*bottom*) for the Co(II) derivatives of OpdA (*filled circle*) and OPH (*open square*). The data were collected in 50 mM, Tris.HCl pH 8.5. Different from OpdA, OPH shows only one protonation event for both k_{cat} and k_{cat}/K_m, whereas two protonation events are discernible from the pH dependence of the k_{cat} of OpdA

pH dependence of the catalytic properties of Co(II)-OPH: comparison to Co(II)-OpdA

The pH dependence of both k_{cat} and k_{cat}/K_m for Co(II)-OPH was measured in the range between pH 5 and pH 11 and compared with the corresponding values for Co(II)-OpdA measured under identical conditions (Fig. 3). The values for Co(II)-OpdA were reported previously by Ely

Table 4 pK_a values for wild-type OpdA with various metal ion compositions, and corresponding metal ion derivatives of OPH

OpdA[a]				OPH[b]	
Metal derivative	pK_{es1}	pK_{es2}	pK_e	pK_{es}	pK_e
Co(II)/Co(II)	4.8 ± 0.1	10.1 ± 0.3	4.8 ± 0.1	7.3 ± 0.1	4.8 ± 0.1
Cd(II)/Cd(II)	4.1 ± 0.1	–	5.3 ± 0.1	8.0 ± 0.1	6.9 ± 0.1
Zn(II)/Zn(II)	4.4 ± 0.1	–	4.9 ± 0.1	5.9 ± 0.1	6.0 ± 0.1

[a] The values for the Co(II), Cd(II) and Zn(II) derivatives of OpdA were taken from Ely et al. [10]

[b] The values for the Cd(II) and Zn(II) derivatives of OPH were from Aubert et al. [12]

et al. [10]. The Co(II) derivatives of both enzymes have a similar maximum k_{cat} value but OpdA is tenfold more efficient (i.e. higher k_{cat}/K_m ratio) than OPH due to better substrate binding. It should be noted that in the previous study the k_{cat} for Co(II)-OPH was reported to be as high as 7,800 s^{-1} [18]. A possible reason for the observed discrepancy is the use of different buffer systems in these two studies; here, a multicomponent buffer system was applied to compare catalytic parameters of OPH and OpdA in an identical environment. In contrast, the former study of Co(II)-OPH used HEPES buffer system. The effect of pH on the catalytic parameters of the two Co(II) derivatives is significant. OpdA is active over a very broad pH range from below 5.0–11.0, whereas OPH gains full activity only at pH values above 7.0. Co(II)-OPH (similar to other metal ion derivatives of this enzyme [12]) has one relevant protonation equilibrium associated with both k_{cat} and k_{cat}/K_m (Fig. 3). The data were fitted using Eq. (5), resulting in $pK_e \sim 6.8$ and $pK_{es} \sim 7.3$. The corresponding values in Co(II)-OpdA differ significantly, with $pK_e \sim 4.8$; for pK_{es} two equilibria are observed, $pK_{es1} \sim 4.8$ and $pK_{es2} \sim 10$ (Table 4) [10].

Effect of increasing substrate concentrations on the catalytic rates

Rate measurements with the substrate paraoxon were carried out with Co(II)-OpdA and Co(II)-OPH using substrate concentrations from 1 to 2,000 μM. While OPH displays Michaelis–Menten-type saturation behaviour, OpdA reaches a rate maximum at a paraoxon concentration of ~400 μM before a gradual decline in the turnover is observed (Fig. 4). This behaviour is characteristic of substrate inhibition, and is observed over a wide pH range. While the data recorded for OPH could be analysed using Eq. (3), a model whereby a substrate molecule can bind to a catalytic and an inhibitory site was employed in the analysis of the data for OpdA (i.e. Eq. 4). The estimated K_i value for paraoxon binding to the inhibitory site is ~1 mM. This rather weak binding may be a reason why in none of the available crystal structures an alternative (inhibitory) substrate binding site has yet been identified. In

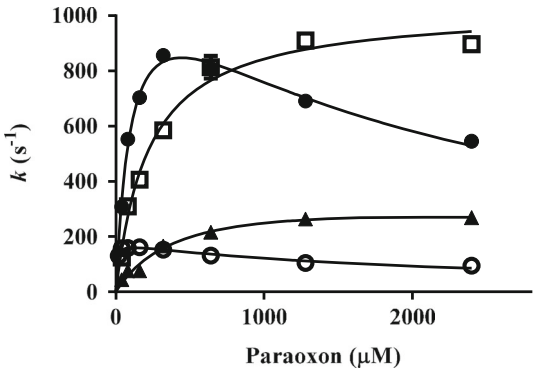

Fig. 4 Effect of the substrate (paraoxon) concentration on the initial rates of the Co(II) derivatives of OPH (*open square*), wild-type OpdA (*filled circle*), the Tyr257Phe OpdA mutant (*open circle*) and the Arg254His OpdA mutant (*filled triangle*). Substrate inhibition is only observed in wild-type OpdA enzyme and its Tyr257Phe mutant. The turnover numbers (k; in s^{-1}) were determined from the specific activities measured by monitoring the initial velocities of product formation as described in the experimental section

an attempt to localize a possible alternative binding site for the substrate residues Arg254 and Tyr 257 in OpdA were mutated to His and Phe, respectively, to disrupt the hydrogen bond network that connects the metal ion centre to the substrate binding pocket (Fig. 1). While the Tyr257Phe mutant of Co(II)-OpdA still displays substrate inhibition (albeit with a greatly reduced rate) the Arg254His mutant obeys Michaelis–Menten-type behaviour (Fig. 4). Thus, the arginine in position 254 is likely to play a relevant role in assisting the binding of inhibitory substrate molecule.

Fluoride inhibition

The inhibitory effect of fluoride was measured for Co(II)-OpdA at pH 6.5, 8.0, and 10.5 (Fig. 5). Data were recorded again with paraoxon as substrate (concentrations ranging from 10 to 2 mM) and different concentrations of fluoride (from 0 to 1 μM NaF). The data were fitted to Eq. (6), resulting in inhibition constants for the competitive (K_{ic}) and uncompetitive (K_{iuc}) modes of fluoride binding,

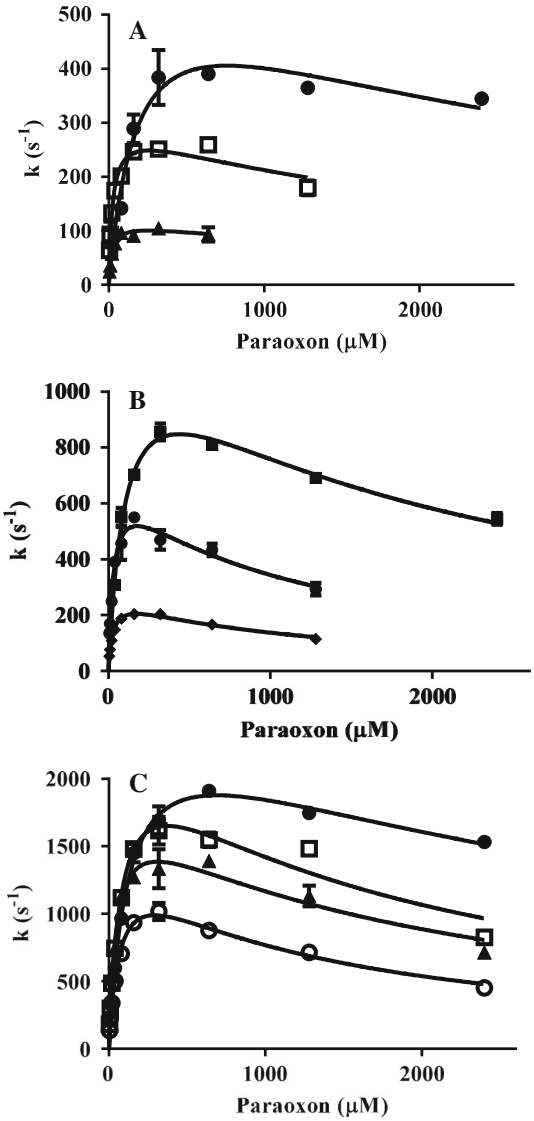

Fig. 5 Inhibition of Co(II)-substituted wild-type OpdA by fluoride. Data were recorded at pH 6.5 (**a**), pH 8.0 (**b**) and pH 10.5 (**c**). Inhibitor concentrations were zero (*filled circle*), 0.1 μM (*open square*), 0.5 μM (*filled triangle*) and 1 μM (*open circle*). The turnover numbers (k; in s^{-1}) were determined from the specific activities measured by monitoring the initial velocities of product formation as described in the experimental section

respectively. Substrate inhibition is apparent at various pHs, and is unaffected by the presence of fluoride. The uncompetitive mode of inhibition is dominant with K_{iuc} being at least ten times smaller then K_{ic} at each pH tested (K_{iuc} = 332 ± 68, 380 ± 56 and 4,315 ± 1,551 nM at pH 6.5, 8.0 and 10.5, respectively). Importantly, the activity of the enzyme is gradually recovered with the increase of the pH. Similar experiments were carried out with the Zn(II) derivative of OpdA and Co(II)-OPH. The former is very strongly inhibited by fluoride over the entire pH range. Since no activity was detectable at fluoride concentration

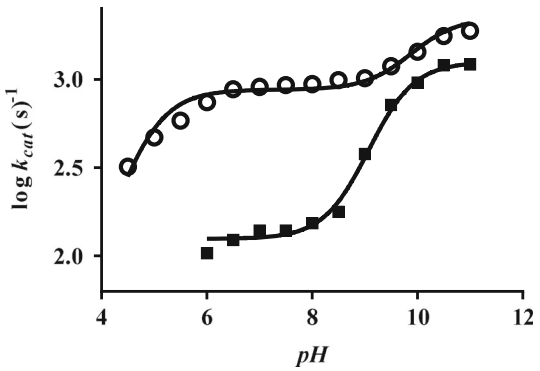

Fig. 6 Effect of pH on the inhibition of Co(II)-OpdA by fluoride. As a control the pH dependence of k_{cat} for the uninhibited enzyme (*open circle*) was reproduced from our previous study (together with the adequate fit to a diprotic model) [10]. For the sample prepared in presence of fluoride (*filled square*) the inhibitor concentration was maintained at 0.5 μM in each assay

as low as 10 nM no attempt to estimate the K_i value was made. In contrast, Co(II)-OPH is not affected by fluoride; even at concentrations as high as 1 mM no reduction in the activity is observed across a broad range of pH.

The pH dependence of the inhibition of Co(II)-OpdA by fluoride is illustrated in Fig. 6. The fluoride concentration was maintained constant at 500 nM and the catalytic rates measured as a function of pH. In the pH range between 6.5 and 8.0 the enzyme was strongly inhibited, but as the pH was increased further the level of inhibition by fluoride sharply decreased. The data were fit to an equation derived for a monoprotic system (Eq. 5), resulting in a pK_a of ~9.5, similar to both pK_a values of water molecules terminally bound to divalent metal ions and pK_{es2} (Table 4).

MCD spectroscopy

MCD spectra of Co(II)-OpdA in the presence and absence of fluoride are shown in Fig. 7a. The spectrum collected without fluoride could be fitted with 13 transitions between 430 and 700 nm. The spectrum of the uninhibited sample was previously shown to be characteristic for a weakly exchange-coupled di-Co(II) centre with a six- and five-coordinate Co(II) species [17]. The assignment of each transition derived from the fitted Gaussians and the AOM calculation for these transitions were reported elsewhere [17]. The MCD spectrum of the same sample after the addition of fluoride displays a very different behaviour, where the MCD bands are quenched indicating strong antiferromagnetic coupling between the Co(II) ions in the dinuclear centre.

The MCD spectrum of Co(II)-OPH containing 2 equivalents of Co(II) displayed four distinct Gaussian-resolved bands corresponding to six- and five-coordinate

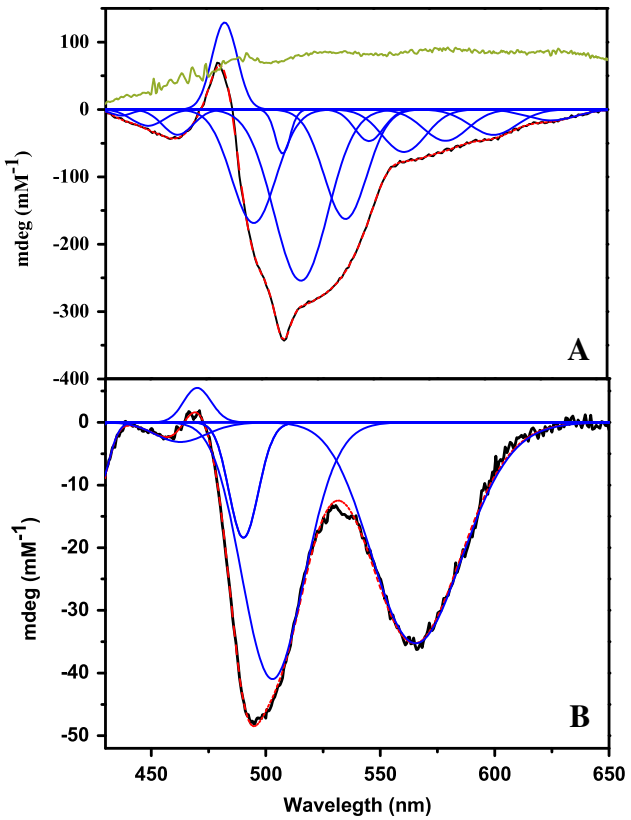

Fig. 7 **a** MCD spectra of Co(II)-OpdA (0.87 mM) in the absence (*red*) and presence (*green*) of 0.5 μM fluoride. The Gaussian fits to the MCD of Co(II)-OpdA in the absence of fluoride is presented in *blue*. The spectra were recorded at 7 T and 1.3 K. The spectrum of the uninhibited sample was Gaussian-resolved and analysed as described in our previous study, and is characteristic of a weakly coupled dinuclear Co(II) system [17]. In contrast, addition of fluoride leads to the formation of a strongly coupled di-Co(II) system; the strong interaction is likely to be mediated via the μ-fluoride group. **b** MCD spectrum of Co(II)-OPH 0.6 mM. Spectrum was fitted to a minimum number of Gaussians which are represented in *blue*. The spectrum was recorded at 1.4 K and 7 T

Co(II) species (Fig. 7b). The assignment of the transitions was assisted by AOM calculations using the AOMX program developed and distributed by Adamansky et al. [31, 32]. The coordinates were based on the Protein Data Bank (PDB) file 1HZY. Each Co(II) metal site was treated separately and the coordinates referred to each metal ion at the origin. The spectrum displayed a strong negative band at 495 nm and two weaker bands, a negative one at 462 nm and a positive one at 470 nm, similar to those reported for a variety of six-coordinated Co(II) complexes [17, 33–37]. The MCD band at 565 nm is consistent in energy to a five-coordinate Co(II) complex [17, 33–36, 38, 39]. The OPH spectrum could be fitted to 5 transitions between 435 and 650 nm (Fig. 7b). Table 5 shows the results for the AOMX calculations based on previous calculations reported for OpdA [17].

Table 5 Summary of the ligand field calculations for Co(II)-OPH using AOMX

Origin in O_h or D_{3h}	*d–d* transition (nm)	
	Observed	Calculated
Six-coordinate		
Origin O_h		
$^4T_{1g} \rightarrow {}^2T_{1g}$ (G)	462	458
$^4T_{1g} \rightarrow {}^2T_{1g}$ (P)	470	472
$^4T_{1g} \rightarrow {}^4T_{1g}$ (P)	490	492
$^4T_{1g} \rightarrow {}^4T_{1g}$ (P)	502	501
Five-coordinate		
Origin D_{3h}		
$^4A_2' \rightarrow {}^4A_2'$ (P)	565	570

AOMX parameters (cm^{-1}): 6-coordinated $\varepsilon_\sigma(H_2O) = 3{,}040$, ε_σ(His 55) = 3,700, ε_σ(Asp 301) = 3,460, ε_σ(Lys 169) = 3,460; 5-coordinated ε_σ(His 201) = 4,790, ε_σ(His 230) = 4,790, ε_σ(Lys 169) = 2,820, $\varepsilon_\sigma(H_2O) = 1{,}490$, B 890, = C = 4.6B

Discussion

Metal ion binding properties of OpdA and OPH

It has been previously shown that for OPH the formation of the dinuclear metal centre is dependent on either the interaction of HCO_3^- or CO_2 with the apo protein prior to metal ion binding [40]. This process, however, takes about 24 h to be completed, which is not suitable for a titration experiment by ITC, where the time scale of the whole experiment is about 2–3 h. The dissociation constants of Zn(II), Co(II) and Cd(II) were thus estimated by competition equilibrium dialysis using the chelator dipicolinate [26, 27, 41]. Here, we used reverse titrations with EDTA to determine the binding affinities of Zn(II), Co(II) and Cd (II) to OpdA (similar data are currently not available for OPH, largely to the low enzyme stability). Similar to OPH, the affinities of the two metal ions in the active site in OpdA differ significantly (Table 3), and the chelation titrations indicate stepwise binding of the metal ions. The magnitudes of the metal ion affinities of OpdA and OPH do not appear to differ greatly (Table 3). However, the low nanomolar K_d values reported for OPH stand in contrast to a recent catalytic study that demonstrated that OPH activity is gradually lost due to a loss of its metal ions, whereas OpdA activity (and metal ion content) remains constant [20]. Thus, despite identical coordination spheres in these two enzymes, amino acid variations in the outer spheres may play a significant role in metal ion binding.

Catalytic properties of OpdA and OPH

The Zn(II) and Cd(II) derivatives of both enzymes, as well as Co(II)-OPH require only one relevant protonation

equilibrium to account for the observed pH dependence of k_{cat} and k_{cat}/K_m. However, as already pointed out in an earlier study [10], OpdA is effective over a considerably larger pH range [10], reflected by pK_a values that are several units lower than those of corresponding OPH metal ion derivatives [10, 12, 16, 18, 42]. Both the pK_a for the free enzyme (pK_e) and the enzyme–substrate complex (pK_{es}) were previously assigned to the metal ion-bridging water molecule [10, 12, 42]. The pH dependence of k_{cat} of the Co(II) derivative of OpdA is more complex, requiring a second protonation equilibrium (pK_{es2}) to account for the increase in reactivity at very high *pH* (Fig. 3) [10]. This pK_a value ($\sim$10) was assigned to a water molecule that is terminally coordinated to one of the Co(II) ions. The mechanistic scheme that emerged from these studies invokes a role of the bridging hydroxide as hydrolysis-initiating nucleophile in the Zn(II) and Cd(II) derivatives of both OpdA and OPH; however, in case of the Co(II) derivative of OpdA the identity of this nucleophile changes as a function of pH, with the terminally coordinated hydroxide replacing the bridging one at high pH [10, 17]. In contrast, in OPH Co(II) does not promote such mechanistic flexibility (its only pK_{es} is similar to that of the other metal ion derivatives of OPH; Table 4).

Of interest is a comparison of the magnitudes of relevant pK_a values since they are a reflection of the active site structures (in particular hydrogen bonding interactions). In general, pK_a values are significantly more acidic in OpdA than in OPH (Table 4). The general assignment of pK_e to the metal ion-bridging water molecule in both enzymes thus implies that factors such as hydrogen bonds are essential contributors in the activation of this nucleophile in OpdA. A major hydrogen bonding interaction is apparent between the bridging water and the α-metal ion ligand Asp301 (Fig. 1), but it is conserved in OpdA and OPH. The increase in acidity in OpdA suggests an additional H-bond interaction in this enzyme alone (not present in other metal derivatives of OPH). A possible candidate is an H-bond between a water molecule terminally coordinated to the β-metal ion and the μ-H_2O. The absence or presence of this terminal water ligand in OpdA could be shown to be associated with the flexibility of Arg254, a second coordination sphere residue lining the substrate binding pocket (Fig. 1) [10]. In wild-type OpdA Arg254 is kept in a rigid (tilted) position away from the β-metal ion via an H-bond with another residue in the substrate binding pocket, Tyr257. Replacement of Tyr257 by a phenylalanine removes this H-bond and allows Arg254 to occupy an additional (elongated) conformation, thereby bringing its guanidinium group in close proximity to the β-metal ion [10]. In this elongated conformation Arg254 effectively lowers the coordination number of the β metal ion by excluding a terminal water ligand, i.e. the water ligand that forms a H-bond with the bridging water molecule. In agreement with this structural observation, the pK_e of Tyr257Phe OpdA is raised to 6.2 [10]. In OPH Arg254 and Tyr257 are replaced by histidine residues and no H-bond network as observed in OpdA is present in the active site (Fig. 1) [10].

From the MCD analysis (Fig. 7), it is apparent that OPH does not display flexibility in the coordination number as observed in OpdA. For the latter MCD together with crystallographic information suggested that the α site is five-coordinate while the β site is predominantly six-coordinate (with small proportion of five-coordinate species). The flexibility in the coordination number of the β site was ascribed to the presence or absence of a terminal water ligand, which is determined by the conformation of residue Arg254 [10]. No crystal structure of the Co(II) derivative of OPH is available. In the structures of the Zn(II)-Cd(II) derivative of OPH the α site appears predominantly five-coordinate while the β site is six-coordinate. It thus seems likely that the Co(II) in the β site also has a terminal water ligand as observed in OpdA, but it may not be forming a hydrogen bond with the bridging water. However, at present it cannot be ruled out that at least in Co(II)-OPH the β site is five-coordinate and the α site six-coordinate. While the two possibilities cannot presently be distinguished it is evident that the immediate coordination environments of Co(II)-OpdA and Co(II)-OPH differ, likely to be due to differences in position 254 of their amino acid sequences.

Investigation of substrate inhibition

The discussion above highlighted the fact that variations in metal ion composition alone cannot account for the mechanistic differences observed between OpdA and OPH. The interaction between the active site and the substrate also plays an essential role in modulating the mechanism of these enzymes. This hypothesis is consistent with the observation that the Co(II) derivatives of OpdA and OPH have similar turnover numbers (k_{cat} values) but different K_m values (Fig. 3) and is further supported by a comparison of the effect of the concentration of the substrate paraoxon on the catalytic rates of these enzymes (Fig. 4). OpdA does not obey Michaelis–Menten behaviour, reaching a maximum rate at a relatively low substrate concentration. A further increase in substrate concentration leads to a reduction in rate, a feature that is characteristic for substrate inhibition. Using Eq. (4), which is effectively an equation describing uncompetitive inhibition, the affinity of the substrate to a second, inhibitory site can be estimated ($K_i \sim 1$ mM). Although this K_i value is considerably larger than the K_m ($\sim$80 μM), the binding of a second substrate molecule to the enzyme–substrate (ES) complex

leads to inhibition of catalysis at sufficiently high substrate concentrations. In contrast, OPH does not display substrate inhibition, obeying Michaelis–Menten-type behaviour (Fig. 4). There is currently no crystal structure depicting the second, inhibitory substrate binding site in OpdA, but since the only variations between this enzyme and OPH are the three amino acid substitutions in the substrate binding pocket that are part of a H-bond network in OpdA but not OPH (see "Introduction") it is plausible that some of these residues are involved in forming a second substrate binding site in OpdA. In a previous study, it was shown that substrate binding to the Tyr257Phe mutant of OpdA partially overwrites the effect of the mutation, evidenced by the similarity of the pK_{es} values of wild-type and mutant form of this enzyme (the pK_e value of the mutant is considerably more alkaline than that of the wild-type enzyme) [10]. Thus, it is not surprising that this mutant also displays substrate inhibition with a similar K_i value ($\sim$1 mM; Fig. 3). More relevant to the observed mechanistic variations between OpdA and OPH may thus be the substitution at position 254 (i.e. from an arginine in OpdA to a histidine in OPH). It was shown that the replacement of His254 by an arginine alters the substrate specificity of OPH to resemble that of OpdA [43]. Similarly, the Arg254His mutation in OpdA alters this enzyme's substrate specificity to resemble that of OPH [10]. The relevance of the residue in position 254 in enzyme–substrate interactions and thus the mechanistic fine tuning in these two bioremediators is further highlighted here by the absence of substrate inhibition in the Arg254His mutant of OpdA (Fig. 4).

Investigation of the effect of fluoride on enzymatic activity

In the above sections, it was illustrated how small variations in the substrate binding pocket have a considerable effect on catalytic properties and substrate specificity of the OP-degrading enzymes OpdA and OPH. However, in terms of reaction mechanism OPH (independent of metal ion composition) and various metal ion derivatives of OpdA are likely to employ the same strategy with a metal ion-bridging hydroxide acting as the hydrolysis-initiating nucleophile [10, 12, 17, 19]. The only exception appears to be the Co(II) derivative of OpdA where the mechanism is proposed to be more flexible since the nucleophile may change its identity depending on pH [10, 17, 19]. In an attempt to substantiate this hypothesis further the effect of fluoride on the enzymatic activity of OPH and OpdA was assessed. Fluoride is a well-known inhibitor of metalloenzymes, including peroxidases [44], laccase [45], ureases [46], arginase [47–49] and purple acid phosphatases (PAPs) [50–52]. In principle, fluoride is able to displace hydroxide ions coordinated to metal ions, and in dinuclear systems there are two binding possibilities, (1) a terminal coordination to one or both of the metal ions, and (2) a metal ion-bridging coordination leading to the formation of a μ-fluoride complex. In arginase fluoride ions bind in both positions [49], while in PAPs the formation of a μ-fluoride complex is prevalent [53, 54]. Since both a terminally bound and a metal ion-bridging hydroxide are proposed as nucleophiles in the Co(II) derivative of OpdA (vide supra) their possible displacement by fluoride may thus provide further insight into the relevant reaction mechanism. At each pH tested a predominantly uncompetitive mode of inhibition is observed. Interestingly, while the Zn(II) derivative of OpdA is very strongly inhibited across the entire pH range, Co(II)-OPH is not affected at all by the presence of fluoride.

To illustrate how pH affects catalysis in Co(II)-OpdA turnover numbers values were determined between pH 6.5 and 11.0 while maintaining the fluoride concentration constant at 0.5 μM. The catalytic activity sharply rises at pH values larger than 9.0 and at pH $\geq$10 the samples with fluoride recovers $\sim$70 % of the enzymatic activity when compared to the samples in the absence of fluoride. The pH dependence of k_{cat} can be fitted to an equation describing the behaviour of a monoprotic system (Eq. 5). The resulting pK_a ($\sim$9.5) is similar to pK_{es2} (Table 4), an acid dissociation constant associated with the terminally coordinated nucleophile in OpdA [10, 17, 19]. For Co(II)-OpdA fluoride inhibition thus supports the mechanistic model whereby the nucleophile alters as the pH is changed. This interpretation is consistent with fluoride binding tightly in a metal ion-bridging mode (low K_{iuc}), but only weakly in a terminal position (high K_{ic}). The binding of fluoride in a bridging mode could be illustrated using MCD spectroscopy. MCD has been employed previously to investigate the mechanism of OpdA and related binuclear metallohydrolases [17, 36]. Here, a spectrum of Co(II)-OpdA was recorded as described previously [17]. The spectrum of the uninhibited sample shown in Fig. 7a is characteristic for a weakly exchange-coupled di-Co(II) centre with a six- and five-coordinate Co(II) species [17]. In contrast, when fluoride is added the transitions disappear. This observation is in agreement with the presence of a strongly antiferromagnetically coupled dinuclear metal ion centre, supporting the replacement of the μ-hydroxo by a μ-fluoride group. It is currently not known why Co(II)-OPH is not inhibited by fluoride but the observation further supports the hypothesis that two enzymes with identical coordination spheres can display significantly functional variations, mediated via amino acid substitutions remote from the metal ion binding sites.

Conclusion

This study has demonstrated that OP-degrading enzymes are not only highly efficient, but also very flexible catalysts. As few as three amino acid substitutions in the vicinity of the active site allows for substantial functional variations in terms of metal ion and substrate preferences, as well as mechanism and inhibition. While this flexibility may have rendered the interpretation of experimental data more challenging, it offers a promising avenue for the application of these enzymes in bioremediation. Only a small number of amino acid variations trigger significant changes in catalytic efficiency as well as substrate and metal ion preference. In particular the residue located in position 254, an arginine in OpdA and a histidine in OPH, is likely to be the crucial mediator for these functional variations. In OpdA, Arg254 may facilitate the binding of a second, inhibitory substrate molecule provided the concentration of this reactant is sufficiently high. Its replacement to a histidine leads to an absence of substrate inhibition. Thus, it is evident that single mutations in organophosphate-degrading enzymes may have significant effects in terms of catalytic properties of these enzymes, an observation that may account for the rapid evolution and adaptation of these enzymes as a response to changing environmental pressures (i.e. pollution) and which may be exploited in the design of derivatives with tailored properties for application in bioremediation.

Acknowledgments This work is financially supported by the Australian Research Council, Discovery Projects Scheme (DP120104263). G. S. also acknowledges the receipt of an ARC Future Fellowship (FT120100694). M. P. is supported by an International Postgraduate Research Scholarship and University of Queensland International Living Allowance Scholarship. J. A. L. and D. E. W. thank the National Science Foundation (USA) for financial support from grants CHE0848433, CHE1303852, and CHE0820965 (MCD instrument) to J. A. L. and CHE1308598 to D. E. W. N. M. would like to thank the Science Foundation Ireland for financial support in form of a President of Ireland Young Researcher Award (SFI-PIYRA).

References

1. Block RM, Dragun J, Kalinowski TW (1984) Groundwater contamination. 2. Health and enviromental aspects of setting cleanup criteria. Chem Eng 91:70–73
2. Dragun J, Kuffner AC, Schneiter RW (1984) Groundwater contamination. 1. Transport and transformation of organic-chemicals. Chem Eng 91:65–70
3. Satoh T, Hosokawa M (2000) Organophosphates and their impact on the global environment. Neurotoxicology. 21:223–227
4. Singh BK, Walker A (2006) Microbial degradation of organophosphorus compounds. FEMS Microbiol Rev 30:428–471
5. McLoughlin SY, Jackson C, Liu J-W, Ollis DL (2004) Growth of *Escherichia coli* coexpressing phosphotriesterase and glycerophosphodiester phosphodiesterase, using paraoxon as the sole phosphorus source. Appl Environ Microbiol. 70:404–412
6. Harper LL, McDaniel CS, Miller CE, Wild JR (1988) Dissimilar plasmids isolated from *Pseudomonas diminuta* MG and a *Flavobacterium sp*. (ATCC 27551) contain identical opd genes. Appl Environ Microbiol 54:2586–2589
7. Yang H, Carr PD, McLoughlin SY, Liu JW, Horne I, Qiu X, Jeffries CMJ, Russell RJ, Oakeshott JG, Ollis DL (2003) Evolution of an organophosphate-degrading enzyme: a comparison of natural and directed evolution. Protein Eng 16:135–145
8. Sutherland TD, Horne I, Weir KM, Coppin CW, Williams MR, Selleck M, Russell RJ, Oakeshott JG (2004) Enzymatic bioremediation: from the enzyme discovery to applications. Clin Exp Pharmacol Physiol 31:817–821
9. Ely F, Foo J-L, Jackson CJ, Gahan LR, Ollis DL, Schenk G (2007) Enzymatic bioremediation: organophosphate degradation by binuclear metallo-hydrolases. Curr Top Biochem Res. 9:63–78
10. Ely F, Hadler KS, Gahan LR, Guddat LW, Ollis DL, Schenk G (2010) The organophosphate-degrading enzyme from *Agrobacterium radiobacter* displays mechanistic flexibility for catalysis. Biochem J 432:565–573
11. Schenk G, Mitić N, Gahan LR, Ollis DL, McGeary RP, Guddat LW (2012) Binuclear metallohydrolases: complex mechanistic strategies for a simple chemical reaction. Acc Chem Res 45:1593–1603
12. Aubert SD, Li Y, Raushel FM (2004) Mechanism for the hydrolysis of organophosphates by the bacterial phosphotriesterase. Biochemistry 43:5707–5715
13. Wu F, Li W-S, Chen-Goodspeed M, Sogorb MA, Raushel FM (2000) Rationally engineered mutants of phosphotriesterase for preparative scale isolation of chiral organophosphates. J Am Chem Soc 122:10206–10207
14. Hong S-B, Raushel FM (1996) Metal-substrate interactions facilitate the catalytic activity of the bacterial phosphotriesterase. Biochemistry 35:10904–10912
15. Raushel FM, Holden HM (2000) Phosphotriesterase: an enzyme in search of its natural substrate. Adv Enzymol Relat Areas Mol Biol 74:51–73
16. Samples CR, Howard T, Raushel FM, DeRose VJ (2005) Protonation of the binuclear metal center within the active site of phosphotriesterase. Biochemistry 44:11005–11013
17. Ely F, Hadler KS, Mitic N, Gahan L, Ollis DL, Larrabee JA, Schenk G (2011) Electronic and geometric structure of the organophosphate-degrading enzyme from *Agrobacterium radiobacter* (OpdA). J Biol Inorg Chem 16:777–787
18. Omburo G, Kuo J, Mullins L, Raushel F (1992) Characterization of the zinc binding site of bacterial phosphotriesterase. J Biol Chem 267:13278–13283
19. Ely F, Pedroso MM, Gahan LR, Ollis DL, Guddat LW, Schenk G (2012) Phosphate-bound structure of an organophosphate-degrading enzyme from *Agrobacterium radiobacter*. J Inorg Biochem 106:19–22
20. Foo J-L, Jackson CJ, Carr PD, Kim H-K, Schenk G, Gahan LR, Ollis DL (2010) Mutation of outer-shell residues modulates metal ion co-ordination strength in a metalloenzyme. Biochem J 429:313–321
21. MicroCal (2004) ITC data analysis in origin—tutorial guide. MicroCalorimeter User's Manual, Northampton
22. Lin LN, Mason AB, Woodworth RC, Brandts JF (1991) Calorimetric studies of the binding of ferric ions to ovotransferrin and interactions between binding sites. Biochemistry 30:11660–11669
23. Lin LN, Mason AB, Woodworth RC, Brandts JF (1993) Calorimetric studies of the binding of ferric ions to human serum transferrin. Biochemistry 32:9398–9406

24. Segel IH (1993) Enzyme kinetics: behavior and analysis of rapid equilibrium and steady-state enzyme systems. Wiley, USA
25. Thermo Scientific, Grams/AI 9.0 Software (2009)
26. Shim H, Raushel FM (2000) Self-assembly of the binuclear metal center of phosphotriesterase. Biochemistry 39:7357–7364
27. Carpenter MC, Wilcox DE (2014) Thermodynamics of formation of the insulin hexamer: metal-stabilized proton-coupled assembly of quaternary structure. Biochemistry 53:1296–1301
28. Grossoehme NE, Spuches AM, Wilcox DE (2010) Application of isothermal titration calorimetry in bioinorganic chemistry. J Biol Inorg Chem 15:1183–1191
29. Sigurskjold BW (2000) Exact analysis of competition ligand binding by displacement isothermal titration calorimetry. Anal Biochem 277:260–266
30. Smith RM, Martell AE, Motekaitis RJ (2004) NIST critically selected stability constants of metal complexes database. Standard Reference Data 46
31. Adamsky H, Schonherr T, Atanasov M (2004) AOMX: angular overlap model computation. Elsevier, Oxford
32. Schonherr T, Artanasov M, Adamsky H (2004) AOMX: angular overlap model computation. In: McCleverty JA, Meyer TJ (eds) Comprehensive coordination chemistry II, vol 2. Elsevier, Oxford, pp 443–455
33. Kaden TA, Holmquist B, Vallee BL (1972) Magnetic circular dichroism of cobalt metalloenzyme derivatives. Biochem Biophys Res Commun. 46:1654–1659
34. Larrabee JA, Leung CH, Moore RL, Thamrong-nawasawat T, Wessler BSH (2004) Magnetic circular dichroism and cobalt(II) binding equilibrium studies of *Escherichia coli* methionyl aminopeptidase. J Am Chem Soc 126:12316–12324
35. Larrabee JA, Alessi CM, Asiedu ET, Cook JO, Hoerning KR, Klingler LJ, Okin GS, Santee SG, Volkert TL (1997) Magnetic circular dichroism spectroscopy as a probe of geometric and electronic structure of cobalt(II)-substituted proteins: ground-state zero-field splitting as a coordination number indicator. J Am Chem Soc 119:4182–4196
36. Hadler KS, Mitic N, Yip SH-C, Gahan LR, Ollis DL, Schenk G, Larrabee JA (2010) Electronic structure analysis of the dinuclear metal center in the bioremediator glycerophosphodiesterase (GpdQ) from enterobacter aerogenes. Inorg Chem 49:2727–2734
37. Hadler KS, Tanifum EA, Yip SH-C, Mitic N, Guddat LW, Jackson CJ, Gahan LR, Nguyen K, Carr PD, Ollis DL, Hengge AC, Larrabee JA, Schenk G (2008) Substrate-promoted formation of a catalytically competent binuclear center and regulation of reactivity in a glycerophosphodiesterase from *Enterobacter aerogenes*. J Am Chem Soc 130:14129–14138
38. Johansson FB, Bond AD, Nielsen UG, Moubaraki B, Murray KS, Berry KJ, Larrabee JA, McKenzie CJ (2008) Dicobalt II/II, II/III, and III/III complexes as spectroscopic models for dicobalt enzyme active sites. Inorg Chem. 47:5079–5092
39. Larrabee JA, Chyun S-A, Volwiler AS (2008) Magnetic circular dichroism study of a dicobalt(II) methionine aminopeptidase/fumagillin complex and dicobalt II/II and II/III model complexes. Inorg Chem 47:10499–10508
40. Hong S-B, Kuo JM, Mullins LS, Raushel FM (1995) CO2 is required for the assembly of the binuclear metal center of phosphotriesterase. J Am Chem Soc 117:7580–7581
41. Kiefer LL, Paterno SA, Fierke CA (1995) Hydrogen bond network in the metal binding site of carbonic anhydrase enhances zinc affinity and catalytic efficiency. J Am Chem Soc 117:6831–6837
42. Samples CR, Raushel FM, DeRose VJ (2007) Activation of the binuclear metal center through formation of phosphotriesterase; inhibitor complexes. Biochemistry 46:3435–3442
43. Grimsley JK, Calamini B, Wild JR, Mesecar AD (2005) Structural and mutational studies of organophosphorus hydrolase reveal a cryptic and functional allosteric-binding site. Arch Biochem Biophys 442:169–179
44. Neri F, Kok D, Miller MA, Smulevich G (1997) Fluoride binding in hemoproteins: the importance of the distal cavity structure. Biochemistry 36:8947–8953
45. Brändén R, Malmström BG, Vänngård T (1973) The effect of fluoride on the spectral and catalytic properties of the three copper-containing oxidases. Eur J Biochem 36:195
46. Todd MJ, Hausinger RP (2000) Fluoride inhibition of Klebsiella aerogenes urease: mechanistic implications of a pseudo-uncompetitive, slow-binding inhibitor. Biochemistry 39:5389–5396
47. Tormanen CD (2003) Substrate inhibition of rat liver and kidney arginase with fluoride. J Inorg Biochem 93:243
48. Pethe S, Boucher JL, Mansuy D (2002) Interaction of anions with rat liver arginase: specific inhibitory effects of fluoride. J Inorg Biochem 88:397–402
49. Cama E, Pethe S, Boucher J-L, Han S, Emig FA, Ash DE, Viola RE, Mansuy D, Christianson DW (2004) Inhibitor coordination interactions in the binuclear manganese cluster of arginase. Biochemistry 43:8987–8999
50. Mitić N, Valizadeh M, Leung EWW, de Jersey J, Hamilton S, Hume DA, Cassady AI, Schenk G (2005) Human tartrate-resistant acid phosphatase becomes an effective ATPase upon proteolytic activation. Arch Biochem Biophys 439:154–164
51. Merkx M, Pinkse MWH, Averill BA (1999) Evidence for nonbridged coordination of *p*-nitrophenyl phosphate to the dinuclear Fe(III), Mn(II) center in bovine spleen purple acid phosphatase during enzymatic turnover. Biochemistry 38:9914–9925
52. Elliott TW, Mitic N, Gahan LR, Guddat LW, Schenk G (2006) Inhibition studies of purple acid phosphatases: implications for the catalytic mechanism. J Braz Chem Soc 17:1558–1565
53. Wang X, Ho RYN, Whiting AK, Que L (1999) Spectroscopic characterization of a ternary phosphatase, substrate, fluoride complex. Mechanistic implications for dinuclear hydrolases. J Am Chem Soc. 121:9235–9236
54. Schenk G, Elliott TW, Leung E, Carrington LE, Mitić N, Gahan LR, Guddat LW (2008) Crystal structures of a purple acid phosphatase, representing different steps of this enzyme's catalytic cycle. BMC Struct Biol 8:6
55. Jackson C, Kim H-K, Carr PD, Liu J-W, Ollis DL (2005) The structure of an enzyme-product complex reveals the critical role of a terminal hydroxide nucleophile in the bacterial phosphotriesterase mechanism. Biochimica et Biophysica Acta (BBA) Proteins Proteomics 1752:56–64
56. Benning MM, Shim H, Raushel FM, Holden HM (2001) High resolution X-ray structures of different metal-substituted forms of phosphotriesterase from *Pseudomonas diminuta*. Biochemistry 40:2712–2722